ELSEVIER

Journal of Fluids and Structures 19 (2004) 171–191

JOURNAL OF FLUIDS AND STRUCTURES

www.elsevier.nl/locate/jnlabr/yjfls

Numerical bridge deck studies using finite elements. Part I: flutter

J.B. Frandsen*

Department of Civil and Environmental Engineering, Louisiana State University, Baton Rouge, LA 70803, USA

Received 26 March 2003; accepted 3 December 2003

Abstract

Wind-induced bridge motions are numerically investigated using structural and fluid finite elements (FEs). The fluid–structure interaction solutions are based on the incompressible Navier–Stokes equations fully coupled to an elastically suspended rigid body. The unsteady fluid field equations with advection-dominated flow are approximated using the weighted residuals method of Galerkin/least squares. The bridge deck is idealized as a lumped mass, spring–dashpot system. The flow simulation around a stationary bridge deck adopts the Eulerian scheme in the entire fluid domain, whereas the simulations of flow past a moving bridge deck apply the arbitrary Lagrangian–Eulerian formulation. Predicting the flutter limit, aiming at reducing the number of physical model tests currently required, is the first step and main objective in the validation of a numerical method applied to long-span bridge decks. It is shown that the low-frequency flexural–torsional flutter motion is the result of a different aerodynamic effect than vortex-induced bridge vibrations. Despite a laminar flow assumption, the two-dimensional self-excited flow solutions, on an irregular unstructured grid of 1884 nodes, predict a flutter limit in good agreement with wind tunnel experiments. The FE model appears to be a suitable method and could be applied as a supplementary tool to wind tunnel testing for the simulation of flutter instability. It was concluded that the prediction of flutter instability for sharp edge bridge decks does not appear sensitive to turbulence and three-dimensional flow structure modelling.

1. Introduction

Design of long-span suspension bridges is governed by wind action. It involves modelling and solving the fluid processes in detail with the structure acting as a moving boundary. The key difficulties with regard to the bridge deck structure is that it is characterized by low structural damping and many modes which are closely spaced at low natural frequencies (<0.3 Hz). Wind-induced phenomena in flexible structures are numerous. They happen at different wind-speed ranges, some of them can occur concurrently and also the different modes of oscillation of the structure may be susceptible to excitation by different mechanisms. Comprehensive backgrounds to the effects of wind on structures are available in the literature [e.g., Simiu and Scanlan, 1996; Dyrbye and Hansen, 1997].

This study is concerned with aeroelastic design considerations related to long-span bridges with a focus on classical flutter. One of the first articles on the theory of suspension bridges was presented by Gilbert (1826). Just after World War II, Selberg (1945) published his book on design of suspension bridges. Approximately 10 years later, Pugsley (1957) published his work on the theory of suspension bridges. Suspension bridges are the type of bridges which can span the greatest distance. Governing design criteria for long-span bridges involve the aeroelastic phenomena of vortex-induced

*Tel.: +1-225-578-0277; fax: +1-225-578-0245.
E-mail address: frandsen@lsu.edu (J.B. Frandsen).

0889-9746/$ - see front matter © 2003 Elsevier Ltd. All rights reserved.
doi:10.1016/j.jfluidstructs.2003.12.005

oscillations, buffeting and flutter (Scanlan, 1981; Dowell et al., 1995). Furthermore, a background to long-span bridge engineering was recently presented by Larsen (1992) and Larsen and Esdahl (1998).

The sharp edges of bluff bodies like bridge decks usually result in a flow less dependent on the Reynolds number (defined as $\mathrm{Re} = UB/\nu$, where U is the free-stream velocity, B is the width of the bridge deck and ν is the kinematic viscosity) effects than the highly Reynolds-dependent flow past circular cylinders. However, the wide decks of long-span bridges result in flow reattachment. Predicting the moving reattachment point on the top and bottom flanges of a bridge deck is an equally challenging problem in comparison with the flow-induced moving separation points on circular cylinders. The Strouhal number, defined as $\mathrm{St} = (n_s D)/U$, where n_s is the shedding frequency, is also an important parameter especially in analyzing vortex-induced oscillations.

Flutter occurs at a high wind velocity (≈ 70 m/s) that has a motion-induced wind load at which the vertical and torsional vibration modes couple. The risk of flutter-induced vibrations is significant when the torsional natural frequency is only slightly larger than the vertical natural frequency, which is usually the case on slender long-span bridge decks. An acceptable flutter limit is one of the principal design criteria for long-span bridges. When the flutter limit is reached the amplitude of vibration rapidly increases causing a bridge to collapse. Scanlan's linearized theory of flutter derivatives (Scanlan and Tomko, 1971), which assumes prescribed motion, is widely used to estimate this. For many decks, especially box-girders, initial estimates of the derivatives may be obtained using Theodorsen's inviscid flat-plate theory (Theodorsen, 1935) and the very useful approximate formula of Selberg (1961). A background to flutter analysis is also given by Fung (1993).

Experimental testing typically reveals a great sensitivity of the bridge behavior to minor changes in leading edge geometry. Such sensitivities cannot be predicted by semi-empirical analytical models such as the lift- and wake-oscillator models (Parkinson, 1989) whose formulation depends on aerodynamic forces obtained from experiments. Moreover, it is not unusual that more than 20 variations of section models are tested in the wind tunnel in order to establish the influence of geometrical modifications of section depth and edge configurations for optimizing the aerodynamic stability. For example, the design of the Great Belt East Bridge involved more than 16 box sections, as described by Larsen and Jacobsen (1992). Each section model test would in average run over 6-weeks. In the initial design phase, this becomes time-consuming and expensive. Numerical solutions are becoming increasingly attractive, not only because they have become affordable, but because they appear to offer increased insight into the complex processes involved in fluid–structure interaction (FSI). This generates hope that the combination of quantitative predictions and improved understanding could lead to more efficient use of experimental facilities, saving expense and time during the design phase by reducing the number of physical model tests required. One long-term goal in the field of bridge aerodynamics is to have a series of numerical methods available to bridge designers to support the conventional wind tunnel tests. This study attempts to investigate the use of fluid and structural finite elements to predict classical flutter. The fluid interaction past two-dimensional (2-D) idealized models are investigated through the arbitrary Lagrangian–Eulerian (ALE) finite-element (FE) method in which the fluid particles are allowed to move independent of the structural motion. The case studies presented are based around the Great Belt East Bridge (Denmark) which is a 4.4 m deep semi-streamlined suspension bridge (Fig. 1). It has a main span of 1624 m and is currently the second largest spanning bridge in the world. Furthermore, unsteady laminar flow models are assumed and no railings are included on the bridge deck model. First, flow is simulated around the bridge deck held in a stationary position. Sensitivity studies

Fig. 1. The box-girder deck of the Great Belt East Suspension Bridge.

on mesh requirement are carried out and the drag/lift forces and Strouhal number are compared with wind tunnel test results. Second, the deck structure is coupled to the fluid model. The first natural frequency, the first torsional frequency and the mass moment of inertia of the full-scale structure are prescribed in order to predict the flutter limit of the bridge. Guide vanes were installed on the bridge to suppress large vortex-induced vibrations experienced full scale (Frandsen, 2001). The article concludes with a case study on FE simulations for a bridge deck with vanes to test their effect on the flutter limit.

The results presented herein have been computed on a single processor workstation with 200 MHz CPU (SPECfp95: 21.4) and 400 Mb RAM of real memory. The FE flutter simulations typically required 3 days of CPU time. The memory was fully utilized for any of the test cases presented.

2. Computational bridge aerodynamics review

The need for numerical models is highly desirable because the high Re present at full scale cannot be reproduced in conventional wind tunnel experiments. Numerical bridge aerodynamics studies is still a young field in computational fluid dynamics research. In the late 1990s a series of publications revealed that significant computational research had begun in this area. In the following, a brief review is given on numerical bridge deck studies. We will learn that the majority of the studies done to model flow around bridge decks numerically include 2-D fluid-only analyses (i.e., flow past stationary decks); both with/without turbulence models. Results from these analyses are typically steady-state coefficients (drag, lift and moment) and Strouhal number. Comprehensive studies have also been carried out on elastically suspended bridge decks which involve analyses with prescribed deck motion allowing linearized aerodynamic motional force coefficients (flutter derivatives) to be determined (Scanlan and Tomko, 1971). The literature also revealed that numerical bridge flutter models usually are 2-D without attempts to include a turbulence model formulation. Other aeroelastic phenomena, for example, buffeting [e.g., Turbelin and Gibert (2002)] and vortex-induced oscillation [e.g., Lee et al. (1995)] have gotten less attention with regard to computational predictions. We note that this does not necessarily imply they are less important. The Re is about a factor 10 lower compared to the flow near the flutter limit. As with other bluff bodies, capturing three-dimensional (3-D) effects and turbulence in the free-stream and in flow instability zones play an important role in replicating these phenomena which in turn make them more difficult to model accurately. Dealing with moderate/high Re naturally raises questions with regard to the importance of modelling three-dimensionality and turbulence. However, accurate flutter predictions appear to be mainly affected by the leading edge separations and the associated pressure forces. Further we note, for sharp leading edges, accurate turbulence modelling and 3-D effects may not be important, whereas it could play a strong role for bridge decks with rounded edges.

One of the first numerical bridge deck simulations relate to the finite-difference method (FDM) and was explored by Fujiwara et al. (1993), both on stationary and moving 2-D grids discretized by 20451 grid points. The Navier–Stokes solutions presented were for Re in the range of 2100 – 4000 following wind tunnel experiments. Onset wind-speed predictions agreed in general with the wind tunnel experiments, but discrepancies were found in the amplitudes, these being overestimated by the numerical model. Fujiwara et al. reported that a possible explanation could be the loss of 3-D effects, the 2-D solution predicting larger fluctuations of lift. Furthermore, Onyemelukwe (1993) developed a 2-D finite difference solver on boundary fitted grids. Laminar Navier–Stokes flow solutions were presented for a variety of fixed bridge decks around Re of 1×10^5. The comprehensive numerical flow visualization studies of Onyemelukwe (1993) were however suppressed by restrictions in CPU and memory. He reported that static force coefficients could not be computed on his IBM 386 PC. It is interesting to note that 10 years after this is no longer a barrier. Later Onyemelukwe et al. (1998) reported on SunSPARC10 simulations but those were related to flow around circular cylinders. In the mid-1990s Kuroda (1997) developed a laminar Navier–Stokes solver discretized also based on the FDM. Solutions for a fixed bridge embedded in an O-grid-type discretized flow domain with 221×101 grid points were shown. Pressure distributions on the deck and static coefficients for Re of 3×10^5 for a range of angle of attacks agreed well with the results of the wind tunnel tests.

Comparable studies to the present FE flutter simulations include the work of Jenssen and Kvamsdal (1999), who uses the finite volume method (FVM) to model the flow field on moving unstructured regular grids. Jenssen and Kvamsdal (1999) show results based on parallel computing techniques. Following the wind tunnel tests and in recognition of inadequate turbulence modelling, the Re was physically incorrect (0.45×10^5) and was kept constant for all wind velocities. The flutter limit was based on 2-D analyses with prescribed deck motions (as opposed to self-excited motions) which was in good agreement with the flutter limit derived from the wind tunnel tests. In contrast to the fully coupled FSI solutions presented in the present simulations, Jenssen and Kvamsdal have a coupling module included in their numerical approach between the FVM fluid solver and an FE structural solver, which resulted in weakly coupled

solutions (as described later in Section 3; also shown in Fig. 5). A background to staggered transient analysis for coupled mechanical system is described in detail by Felippa and Park (1980). Furthermore, Jenssen and Kvamsdal (1999) are currently one of the few researchers who have done numerical bridge studies on 3-D flow models. Their investigations include large eddy simulations on stationary grids expanding a 2-D model of 75 000 cells to $40 \times 75\,000$ cells over a distance of $0.2 \times$ B (where B is the width of the bridge of 31 m) along the span, from which they conclude that the pressure distribution, the steady state lift and pitching moment are in closer agreement with the results of the wind tunnel [see also Jenssen, 1998]. However, the present investigations indicate that it does not appear evident that models of this size are required nor that 3-D simulations are required for the flutter limit prediction as 2-D coarse models ($\approx$1900 nodes in an irregular unstructured grid) without boundary layer modelling seems sufficient, as shown later in Section 5.

Other investigators have also used and developed FVM solvers. For example, De Foy (1998) applied his unsteady incompressible finite volume solver to the Great Belt East bridge deck section. Fluid-only simulations in 2-D were performed for a Re of 1.38×10^8; assuming laminar flow. De Foy found an St = 0.17 which compares reasonable well with the section model of the wind tunnel (0.11–0.15), where Re was in the order of 0.4×10^5 to 1.5×10^5. Furthermore, Bruno et al. (2001) applied the FVM which includes a k–ε-model when solving the flow past the complicated leading edge detail (including railings) of the Normandy cable-stayed bridge (France). Using parallel computations, Bruno et al. (2001) present 2-D flow results for the stationary bridge deck. Their optimized fluid model consist of an unstructured irregular grid with domain size of $50B \times 40B$. The fluid domain is discretized by 29 000 nodes with a cell thickness at the wall of $2 \times 10^{-3}B$, where the width of the bridge deck, $B \approx 21.2$ m. They reported good agreement with the wind tunnel results when comparing force coefficients for the fixed bridge deck.

Previous numerical studies using the FE method have been undertaken by, e.g., Lee et al. (1995), Mendes and Branco (1998) and Selvam et al. (2002). Lee et al. (1995) modelled FSI through moving structured regular grids adopting the ALE formulation. Their 2-D fluid model included a k–ε-model and a streamlined-upwind Petrov Galerkin (SUPG) approximation was assumed. Lee et al. (1995) explored the use of this FE approach on several bridges. The static force coefficients agreed with the results obtained in the wind tunnel but some discrepancies were found with regard to the onset velocity of vortex-induced resonance. Mendes and Branco (1998) carried out flow investigations on the Vasco da Gama cable-stayed bridge (Portugal). They assumed laminar flow. However in recognition of the high prototype Re, an incorrect low value of Re (3×10^3) was used in the demonstration of the flow solutions. For this flow regime, their studies demonstrated that a cross-section with baffles aids the suppression of torsional instability. Furthermore, Selvam (1998) developed an FE model on a rotating moving frame of reference. Their FE model was to the approach bridges of the Great Belt East (Denmark) and, in a more recent analysis, to the main suspension bridge (Selvam et al., 2002). Selvam et al. present large eddy simulations for an Re in the order of 10^5. In their recent analysis they use structured regular grids of 14 805 nodes contained within a control volume $3B \times 8B$. They report on drag coefficients and the flutter instability limit which are in agreement with the wind tunnel tests.

In recent years the spectral method, described by Karniadakis and Sherwin (1999), has made interesting contributions to modelling moving boundaries. A main advantage is resolving the steep boundary layer gradients and shear layers with high-order resolution. Spectral element methods also allow for advecting the flow structures with greater accuracy similar to the vortex methods described below. Using spectral elements also seem to be less CPU demanding compared to the ALE approach. Li et al. (2002) developed and applied their spectral method based on a rotating moving frame of reference. In a 2-D case study, they applied their model to predict the flutter limit of the Second Forth Road Bridge, UK (Robertson et al., 2003b). The computational irregular unstructured mesh was made up of 1789 elements and Re ranged between 4167 to 11 667. Good agreement with wind tunnel tests were found although the physical small-scale experiments were based on Re in the order of 1×10^5 to 1×10^6. Futhermore, the spectral method of Li et al. (2002) was also applied to explore the single degree of freedom instability problem of galloping of bluff bodies, e.g., Robertson et al. (2003a). Recent investigations provide more detail on bridge deck behavior, as described by Robertson et al. (2003c).

Grid generation (even in 2-D) can be a time-consuming process, especially when the grids involve bluff bodies. To this end, avoiding the use of grids, the discrete-vortex method (DVM) pioneered in the 1960s by Sarpkaya and Chorin as described in the comprehensive reviews [e.g., Sarpkaya (1989), Chorin (1989)], is attractive for FSI analysis. DVM has been popular for many decades (Leonard, 1980). In particular, the method of source panels has been used for studying aerodynamic interactions among various components of an aircraft. The vortex elements are naturally concentrated into areas of nonzero vorticity and unlike the grid-based methods, this means that the small-scale flow structures will automatically be captured. However, DVM developers are faced with other difficulties in that several parameters must be prescribed, such as the core radius, defining the maximum circulation to be released for one boundary element and at which distance the surface vorticity is to be released from the bridge surface. The 2-D DVM has been applied to bridge decks by, e.g., Walther (1994), Morgenthal and McRobie (2002), Taylor and Vezza (2002).

In a series of publications, e.g., Walther and Larsen (1997) show flow solutions for fixed bridge decks and flutter limit predictions in agreement with wind tunnel results. Taylor and Vezza (2002) have also developed a DVM solver and present results on stationary and oscillating bridge decks. The derived flutter limit based on prescribed motion compare well with wind tunnel tests. In addition, they show extensive investigations of the flutter motion being suppressed by inclusion of active control vanes.

Finally, it should be mentioned that various investigators have used hybrid models. For example, Brar (1997) developed a coupled finite-difference and vortex-method scheme. An Eulerian finite-difference grid was located in the viscous region next to the bluff body section and the Lagrangian vortex element domain in the flow regions away form the wall boundaries. Flow solutions were presented for Re of 100–1000. St predictions agreed in general with the solutions of others. In some case, the numerical solution overpredicted the St.

This present paper explores the use of a fully coupled FE FSI solver to simulate (1) flow past a fixed deck and (2) to predict the self-excited flutter instability limit.

3. The FE formulation

The numerical solutions of the convection-dominated flow are obtained from a semi-discrete FE formulation of the flow field equations assuming isothermal incompressible viscous flow contained within the multiphysics FE code *Spectrum* (Ansys Inc., 1999). A brief theoretical background of *Spectrum* is presented here and is limited to the context of the application to long-span bridge aeroelasticity. To the knowledge of the author, this is a new application of *Spectrum*. The most closely related work is the project of Okstad and Mathisen (1998) and Remseth et al. (1999). They used *Spectrum* to carry out the FSI simulations for a Reynolds number of 12 812 on a submerged road bridge. They showed results from 2-D simulations of water flow past an elastically suspended circular cross-section. The cylinder displacements agreed quantitatively well with the water-tank experiments reported in Dahle et al. (1990). Okstad and Mathisen (1998) also concluded that the FSI simulations indicated a larger dependency on the FE mesh than the corresponding fixed cylinder case. Although difficulties in the numerical experiments were experienced, these were mainly due to the free surface behavior, and thus not particularly relevant to the bridge aerodynamic problem.

In this study, investigations into the FSI mechanisms due to wind action on either a stationary or a moving long-span bridge deck are carried out. The FE model of this coupled FSI problem consists of three main regions: (i) the fluid domain where the incompressible Navier–Stokes equations (NSEs) are to be solved; (ii) the structural domain where nonlinear elasticity equations are to be solved; and (iii) the interface region. For this application the mathematical formulation strongly couples the incompressible isothermal Navier–Stokes equations of the fluid to the structural equations. This is achieved by means of an ALE formulation, where the FE mesh is allowed to move independently of the motion of the fluid particles themselves. The numerical results presented herein are based on 2-D models. For the FE theory however, the third dimension does not complicate the formulation and no such restriction is imposed.

3.1. Fluid domain

The flow regimes of interest in bridge aerodynamics occur with maximum wind speeds of around 70 m/s. This is equivalent to a Mach number much less than one; thus, it is assumed that the flow is incompressible for wind-induced bridge motions. The governing equations of motion are the incompressible isothermal NSEs described (gravity term here excluded) by

$$\mathbf{u}_t + (\mathbf{u}\cdot\nabla)\mathbf{u} = -\frac{1}{\rho}\nabla p + \nu\nabla^2\mathbf{u}, \tag{1}$$

and the continuity equation,

$$\nabla\cdot\mathbf{u} = 0, \tag{2}$$

where the gradient operator is defined as

$$\nabla = \frac{\partial}{\partial x}\mathbf{i} + \frac{\partial}{\partial y}\mathbf{j} + \frac{\partial}{\partial z}\mathbf{k}. \tag{3}$$

The dependent variables are the pressure p, and the fluid particle velocity vector $\mathbf{u} = \{u, v, w\}^{\mathrm{T}}$ with reference to x, y and z Cartesian directions, where $\mathbf{i}$, $\mathbf{j}$ and $\mathbf{k}$ are unit vectors. The fluid flow is assumed to be laminar and Newtonian. We assume a constant air density $\rho = 1.23\ \mathrm{kg/m^3}$. The kinematic viscosity ν ($= \mu/\rho$, where μ is the dynamic viscosity) is assumed constant with a value of $1.5\times10^{-5}\ \mathrm{m^2/s}$ for air at 20°C.

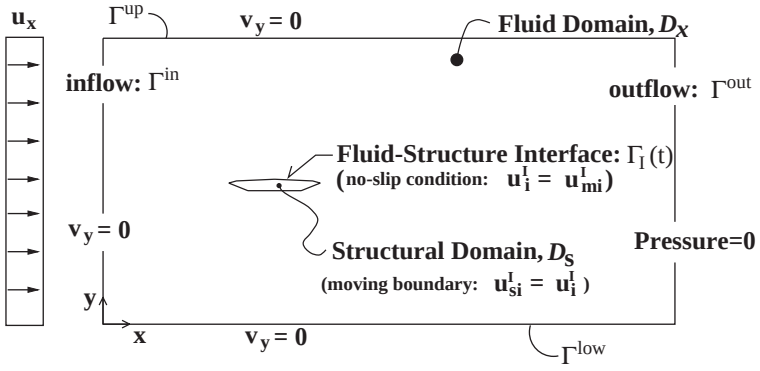

Fig. 2. Domains and fluid–structure interaction boundary conditions.

The unsteady laminar equations with advection-dominated flow are modelled using the weighted residuals method of Galerkin/least squares (GLS), as described by Hughes et al. (1989) in which residuals of the Euler–Lagrange equations have been appended in least squares form to the standard Galerkin projection. The GLS method extends the idea of the SUPG formulation. The idea originates from the early work of Hughes and Brooks (1979).

To obtain a unique solution for the governing equations, it is necessary to specify initial and boundary conditions. For the transient analyses herein, the initial conditions are typically set (somewhat arbitrarily) to the free-stream velocity and zero pressure throughout the domain. A more realistic flow usually appears after several seconds of real-time simulation; that is, letting the process settle for a while until an arbitrary particle has gone through the computational domain once or twice.

The boundary conditions for the fluid domain are shown in Fig. 2. The fluid domain D_x is surrounded by boundaries $\mathbf{\Gamma}^{\text{up}}$, $\mathbf{\Gamma}^{\text{low}}$, $\mathbf{\Gamma}^{\text{in}}$ and $\mathbf{\Gamma}^{\text{out}}$ fixed in space, all specified as rigid boundaries, i.e., zero mesh velocity at these boundaries ($u_{mi} = 0$). The boundary $\mathbf{\Gamma}_I$ denotes the moving interface between the fluid and the structural domains. The fluid particle velocity, mesh velocity and structural velocity are denoted u_i, u_{mi} and u_{si}, where in 2-D $i = \{x, y\}$ denotes the horizontal and vertical directions. Constant velocity at the inflow is assumed, as shown in Fig. 2, i.e., no turbulence is included in the incoming mean wind speeds. Furthermore, for flow past a fixed bridge deck, there is no mesh motion specified at the interface, i.e., $u^I_{mi} = 0$ (and likewise in the entire fluid domain). The boundary conditions are here divided into nodal boundary conditions (acting on $\mathbf{\Gamma}^{\text{up}}$, $\mathbf{\Gamma}^{\text{low}}$, $\mathbf{\Gamma}^{\text{in}}$) and element boundary conditions at the outlet, $\mathbf{\Gamma}^{\text{out}}$. The nodal boundary conditions (Dirichlet conditions) are applied on the three fluid boundaries as specified in Fig. 2:

(i) *inflow boundary*: prescribed free-stream velocity, u_x and $v_y = 0$; mesh movement is constrained, ($u_{mi} = 0$) on $\mathbf{\Gamma}^{\text{in}}$;
(ii) *upper and lower domain boundaries*: tangential slip $v_y = 0$; mesh movement is constrained, ($u_{mi} = 0$) on $\mathbf{\Gamma}^{\text{up}}$, $\mathbf{\Gamma}^{\text{low}}$;
(iii) *entire fluid domain in 2-D analyses*: out-of-plane fluid particle velocity, $w = 0$; out-of-plane mesh velocity, $w_m = 0$.

The element boundary conditions (Neumann conditions) are applied only at the outlet. Here we prescribe zero outlet pressure $p = 0$, and tangential tractions, $t_i \equiv \tau_{ij} n_j$ on $\mathbf{\Gamma}^{\text{out}}$, where n_j is the unit outward vector normal and τ_{ij} is the 3×3 viscous stress tensor defined as $\tau_{ij} = 2\mu\, u_{i,j}$. The mesh movement is also constrained. Note that $p = 0$ on $\mathbf{\Gamma}^{\text{out}}$ is legitimate only if the outlet boundary is far enough from the bridge deck. For the case studies herein this distance is equivalent to four times the width of the bridge deck (measured from the tip of the trailing edge).

3.2. Structural domain

The structure considered is essentially 2-D, and is mounted on elastic springs with viscous dashpots appropriate to the structural mode of vibration under consideration. In effect, the structure is modelled as an elastic boundary condition embedded within the fluid domain. On this boundary, structural elements are attached to model a rigid bridge deck. The structural equations of motion for the dynamical behavior of a damped linear mechanical system with n degrees of freedom are

$$\mathbf{M}_s \mathbf{u}_{si,t} + \mathbf{C}_s \mathbf{u}_{si} + \mathbf{K}_s \mathbf{x}_{si} = \mathbf{F}_{si}, \tag{4}$$

where $\mathbf{M}_s$, $\mathbf{C}_s$ and $\mathbf{K}_s$ denote the mass, damping and stiffness matrices, and $\mathbf{x}_{si}$ and $\mathbf{F}_{si}$ the displacements and fluid forces. The subscript $i = \{x, y, \theta\}$ denotes the horizontal, vertical and rotational directions. The right-hand side of Eq. (4)

contains the resultants of the surface traction of fluid. Further we note that the fluid velocity is identical to the structural velocity (u_{si}) at the interface due to the specified no-slip condition. The matrix contents of $\mathbf{M}_s$, $\mathbf{C}_s$ and $\mathbf{K}_s$ depend on whether the simulations are vortex-induced oscillations or flutter. In the flutter simulation, the vertical and rotational degrees of freedom couple and off-diagonal terms are included in the matrices. If large rotations occur during these simulations, extra stiffness terms are automatically generated through nonlinear specification in *Spectrum*. Using special lumped elements (in user-defined functions), stiffness and damping are specified through springs and dashpots and the mass is lumped. The *Spectrum* program was developed for 3-D models and therefore does not offer an interface between structural beam elements and fluid shell elements. Instead the structural elements are modelled using four-node quadrilateral elements, which are given an artificial high stiffness to simulate rigid bridge deck boundaries together with specified zero continuous mass. The fluid domain contains either eight-noded hexahedral or six-noded triangular prism elements. The major drawback of using *Spectrum* for 2-D modelling is a model which contains twice the numbers of nodes intended and therefore double the amount of equations to be solved.

The no-slip condition is prescribed along the fluid–structure interfaces. This means that the following velocity condition must be satisfied,

$$\mathbf{u}_{si}^{I} = \mathbf{u}_{i}^{I} \quad \text{on } \Gamma_I, \tag{5}$$

where $\mathbf{u}_{si}$ and $\mathbf{u}_i$ represent the velocity fields of the structure and the fluid particles, respectively.

In addition to the kinematic boundary conditions, it is also necessary to impose continuity of traction at the fluid–structure interfaces,

$$\boldsymbol{\tau}_{s}^{I} = \boldsymbol{\tau}_{ij}^{I} \quad \text{on } \Gamma_I. \tag{6}$$

A plane-strain condition is used to simulate the structural domain (D_s) in 2-D, i.e., the nodal boundary condition set for all nodes of the deck is defined to consist of zero out-of-plane displacements and zero x- and y-rotations.

3.3. The fluid – structure interface

Most fluid FE analyses are accomplished using the Eulerian description in which the mesh is fixed in space and the material particles flow through the mesh, as shown in Fig. 3(a). Each FE is crossed by the fluid flow. In an aeroelastic analysis, the Eulerian description is inadequate as the domain surrounding the structure is itself in motion. The usual numerical representation for structural motion is the Lagrangian description in which the mesh motion coincides with the motion of the material particles, as illustrated in Fig. 3(b). The fluid domain is free to move, but the mesh movement and the velocity of the fluid particles are constrained to be the same. This may result in severe mesh distortions due to, for example, vortex-induced oscillations as each element always contains the same fluid particles. The ALE approach, supported by the general kinematic theory in Hughes et al. (1981), provides a method for the solution of the equations describing fluid flow through a moving mesh, as shown in Fig. 3(c). The nodes of the mesh are free to move independently of the fluid flow. The concept of the moving and deforming reference frame (ALE) has been introduced in finite differences by Noh (1964). Later, it was implemented in FEs by Donea et al. (1977). In the ALE scheme, the convective term in the NSEs contains the relative velocity between particles and mesh. The specific application of the ALE scheme to a moving bridge deck is illustrated in Fig. 4. No deforming fluid domain boundaries are specified in the current FSI analyses, and the bridge deck is kept as a moving rigid body.

In the present work flow simulation around a stationary bridge deck adopts the Eulerian scheme in the entire fluid domain, whereas the simulations around a moving bridge deck adopt the ALE scheme in the whole fluid domain. Several investigators, among these Anju et al. (1997), Mendes and Branco (1999) and Nomura and Hughes (1992), have described a way of reducing computations by having only a small part of the mesh around the structure as a moving ALE mesh, and the nonadjacent fluid mesh following the standard Eulerian scheme.

The mesh motion is solved as a quasi-static problem from

$$\mathbf{K}_m \mathbf{x}_{mi} = \mathbf{F}_{mi}, \tag{7}$$

where $\mathbf{K}_m$ is the stiffness matrix which depends on the mesh movement $\mathbf{x}_{mi}$, if large deformations are encountered. The subscript $i = \{x, y, \theta\}$ denotes horizontal, vertical and rotation. We note the inertia and damping terms are not actually included in the solution process. It should be emphasized that the mesh formulation has no physical interpretation, i.e., terms such as Cauchy stresses and elastic moduli do not have the usual physical interpretation within this context. In effect, the mesh is modelled as an elastic solid, whose interior node positions are computed as if all nearest nodal neighbors were coupled by an elastic medium and which sets the positions and velocities of the boundary nodes to precisely match the boundary motions. In reality, it is a purely mathematical construct, i.e., a method for updating the mesh in such a way that it maintains integrity. Note that the model does not absolutely guarantee mesh integrity, as it

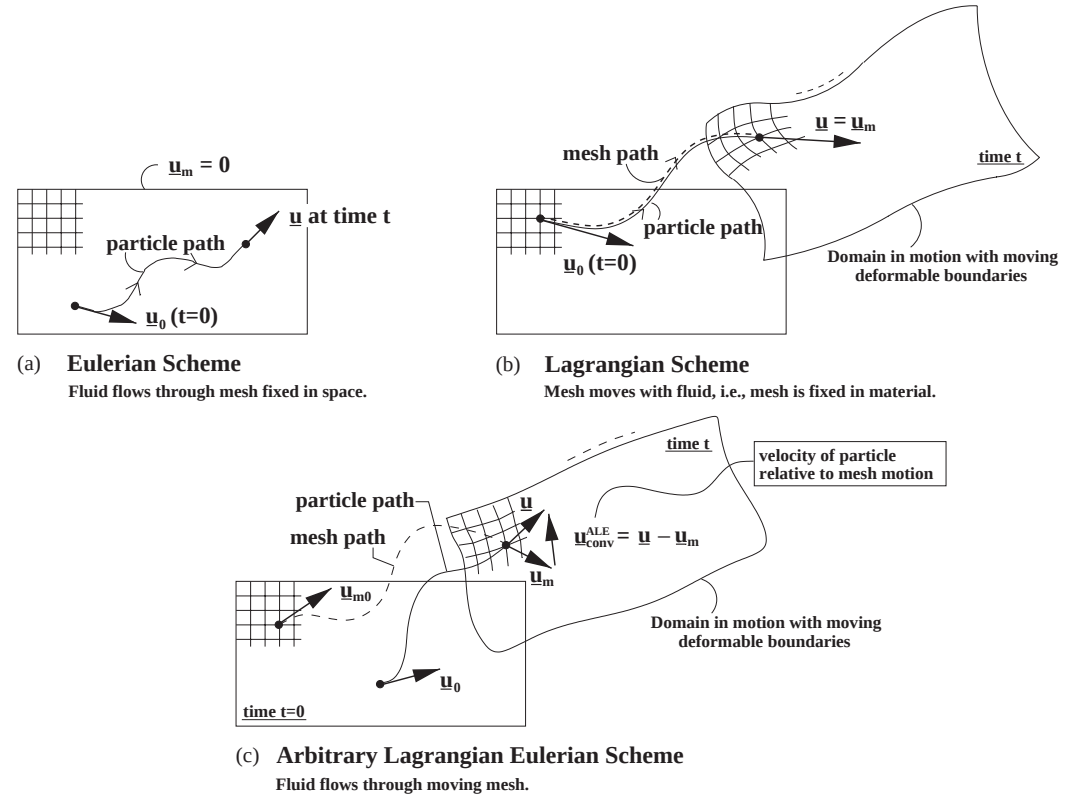

Fig. 3. FE schemes: (a) Eulerian scheme, (b) Lagrangian scheme and (c) ALE scheme.

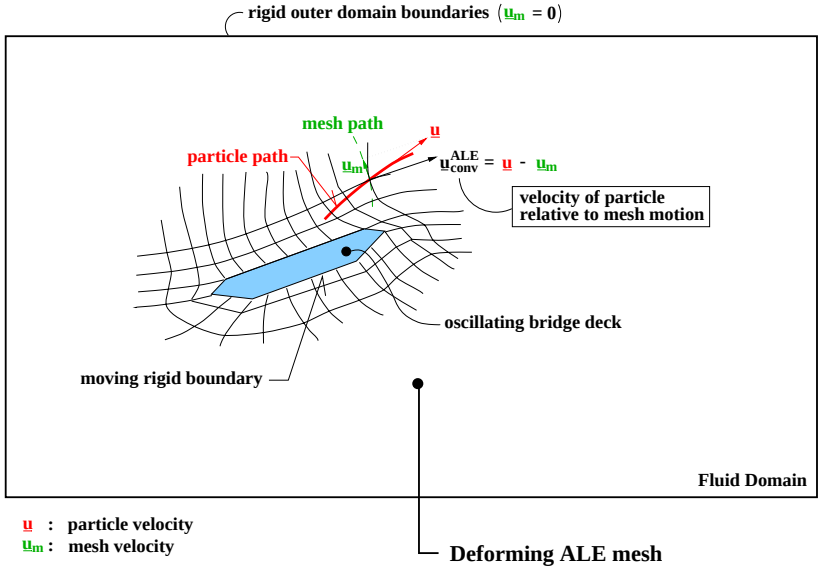

Fig. 4. The ALE scheme applied to a wind-induced moving bridge deck.

may be violated if very large deformations or twisting motions are simulated. In such cases, the problem must be remeshed.

The boundary conditions for the FSI analyses are shown in Fig. 2. The domain D_s is the moving idealized rigid bridge deck supported on elastic springs, and D_x is the moving spatial domain of viscous incompressible fluid elements over which the fluid motion is described. For the FSI analyses, further boundary conditions are specified in the mesh equations to keep the fluid mesh in contact with the moving structure. It is through the specification of compatibility and equilibrium at the interfaces the fluid and the moving structure is achieved. Only a compatibility condition is imposed on the mesh equations, i.e., the mesh follows the structure and fluid interfaces.

At the interfaces, continuity of displacement, velocity and traction fields must be satisfied for all times at all points on the boundary Γ_I, where I denotes the interface. This leads to the following boundary conditions on the interfaces:

- *coupling of displacement fields*: the structure and the mesh displacements need to satisfy

$$\mathbf{x}_{si}^I = \mathbf{x}_{mi}^I \quad \text{on } \Gamma_I^{\text{mov}}(t), \tag{8}$$

  such that the boundary of the fluid mesh follows the motion of the structure.
- *coupling of velocity fields*: the fluid and the mesh velocities needs to satisfy

$$\mathbf{u}_i^I = \mathbf{u}_{mi}^I \quad \text{on } \Gamma_I^{\text{mov}}(t), \tag{9}$$

where $\mathbf{u}_i^I$ is the fluid particle velocity and $\mathbf{u}_{mi}^I$ is the velocity at the moving interface $\Gamma_I^{\text{mov}}(t)$ imposed because of the no-slip condition on $\Gamma_I^{\text{mov}}(t)$. This boundary condition is equivalent to having a Lagrangian description on Γ_I.

In *Spectrum*, the boundary conditions are transformed into a set of constraint equations. These equations are added to the system equations and enforced through a set of Lagrange multipliers ensuring that the fluid always stays in contact with the structure.

Knowing the entire set of boundary conditions, the coupled equations can now be solved,

$$\begin{aligned} &\mathbf{u}_{i,t} + ((\mathbf{u}_i - \mathbf{u}_{mi}) \cdot \nabla)\mathbf{u}_i = -\frac{1}{\rho}\nabla p + v\nabla^2 \mathbf{u}_i, \quad \nabla \cdot \mathbf{u} = 0, \\ &\mathbf{M}_s \mathbf{u}_{si,t} + \mathbf{C}_s \mathbf{u}_{si} + \mathbf{K}_s \mathbf{x}_{si} = \mathbf{F}_{si}, \\ &\mathbf{K}_m(\mathbf{x}_{mi})\mathbf{x}_{mi} = \mathbf{F}_{mi}. \end{aligned} \tag{10}$$

The right-hand side of the structural equation of motion in Eq. (10) contains the resultants of the surface traction of the fluid. Note also that the interface fluid velocity is a function of the velocity of the structure, $\mathbf{u}_{si}$, as described in Eq. (5). In summary, the system equations represent a structural response ($\mathbf{x}_{si}$) whose magnitude depends on the fluid pressures acting on it. In turn, the movement of the fluid mesh ($\mathbf{x}_{mi}$) depends on the structural motions ($\mathbf{x}_{si}^I$) at the interface. The motion of the mesh in the fluid domain affects the convection term of the fluid equations through the mesh velocity ($\mathbf{u}_{mi}$) affecting fluid pressures.

The coupled Eqs. (10) together with the interface constraints and boundary conditions, are recast in a matrix form. The resulting system of ordinary differential equations in time is then solved. The *Spectrum* Code employs a multistagger approach, which partitions the full system of coupled field equations into two or more smaller equation subsystems (staggers). For flow past a stationary bridge deck, the field equations are solved for velocities and pressures only. These unsteady fluid-only models are solved using a segregated stagger approach within each time-step, assuming a weak coupling between the velocity (stagger 1) and the fluid pressure (stagger 2); i.e., one solves for the velocity while keeping the pressure frozen and then solving for the pressure with the new velocities held constant, etc. The velocity and pressure stagger are solved implicitly (Hilber et al., 1977) using iterative solvers, that is, the conjugate gradient solver for the pressure stagger (symmetric matrix problem) and the generalized minimum residual for the velocity stagger (nonsymmetric matrix problem). When monitoring the convergence criteria, it is typically observed that the pressure convergence takes more nonlinear iterations before stabilizing compared to the convergence of the velocities.

Solutions for the FSI problem are achieved through a strong coupling between fluid velocity/pressure and structural displacements (stagger 1) weakly coupled to the fluid mesh displacements (stagger 2). In a first set of iterations, the fluid velocity/pressure (stagger 1) is found causing a change in the geometry as a result of the fluid mesh moving (stagger 2). The fluid velocity/pressure values are updated to accommodate the new geometry and the converged new set of fluid velocity/pressure values will again satisfy the field equations. Having updated the velocities and the pressures on the fluids, the load on the structure (stagger 1) has changed and as a result the structure moves. To accommodate the displacements, the fluid mesh needs to update itself (stagger 2). The process repeats itself in the stagger control loop until convergence at both staggers are reached before moving on to the next time step, achieving the time-accurate solution for a fixed time increment within each time step. The velocity and pressure stagger are solved implicitly as for

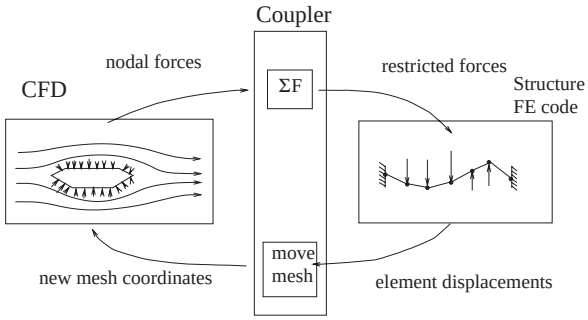

Fig. 5. Alternative FSI system, after Kvamsdal et al. (1999).

the fluid-only problem, but using sparse direct solvers as opposed to the iterative solvers used for the fixed bridge deck case. In FSI analyses, the use of the iterative solver introduces ill-conditioning in some cases, resulting in the lack of robustness. The sparse direct solvers do not suffer from this lack of robustness. Monitoring the convergence criteria in the FSI analyses involves many more subsets of iterations compared to the fluid-only analyses, but the convergence of the state variables compared to the residual convergence nevertheless dominates in the convergence loops.

Furthermore, it should be mentioned that the *Spectrum* code used as a tool for all the numerical FE experimentation in this paper was distributed for commercial use in 1993–1999. It differs from other FE software in the fact that it is able to perform fully coupled fluid–structure analyses. This is in contrast with the more traditional approach where a weakly coupled method is used, as shown in Fig. 5, by repeatedly solving the fluids and solids problem separately and exchanging the results of one analysis as initial conditions for the next (Kvamsdal et al., 1999).

4. Flow past a stationary bridge deck

In the case studies presented in the following section, prior to the full fluid–structure analyses of moving bridge decks, a series of simulations are undertaken to observe the unsteady flow patterns around a stationary structure in an attempt to establish mesh-modelling criteria for the flow phenomena of interest. The solution of the fluid equations results in computed pressures and tractions which act on the bridge. The resulting forces on the bridge deck are then computed by integrating the pressures and friction components along the boundary on the deck surfaces. The net forces (per unit span) are usually expressed in a dimensionless form, and referred to as the aerodynamic coefficients, the drag (C_D), the lift (C_L) and the moment (C_M) coefficients:

$$C_D(t) = \frac{F_D(t)}{\frac{1}{2}\rho U^2 D}, \quad C_L(t) = \frac{F_L(t)}{\frac{1}{2}\rho U^2 B}, \quad C_M(t) = \frac{M(t)}{\frac{1}{2}\rho U^2 B^2}, \tag{11}$$

where U is the free-stream velocity, B; D is the width and depth of the bridge deck, and F_D; F_L, and M are the drag, the lift and the moment coefficients. The drag contains contributions from both skin friction drag and pressure drag, the former being the along-wind resultant of the shear stresses acting tangential to the deck surfaces and the latter the along-wind resultant of the pressures acting normal to the deck surfaces. The lift is the fluid force exerted on the bridge perpendicular to the flow direction, containing pressure and friction contributions. Lift occurs on a bridge deck mainly due to differences in pressures between top and bottom flanges.

Based on initial studies, a minimum fluid domain of 100×200 m^2 with an arbitrary depth of 1 m was adopted, surrounding the 31 m wide, 4.4 m high suspension bridge box-girder deck. The fluid domain is discretized using one layer either of eight-noded hexahedrons or six-noded triangular prism elements. Both element types have linear variation for velocities and piecewise constants for pressures. The flow regimes for these fluid analyses are in the region $6.2 \times 10^6 < \mathrm{Re} < 1.65 \times 10^7$ corresponding to a full-scale velocity range 3 – 8 m/s. Note that 8 m/s is the wind speed where large vortex-induced oscillations were observed and recorded full scale (Frandsen, 2001).

As mentioned these investigations are limited to idealized 2-D flow. All analyses undertaken herein are for unsteady laminar flow. Some large eddy simulations based on the Smagorinsky model (Smagorinsky, 1993) were carried out by Frandsen (1999) but are not presented herein as this model improvement has no effect on the flutter limit prediction. As we will learn the prediction of flutter instability for sharp edge bridge decks does not appear sensitive to turbulence and 3-D flow structure modelling Furthermore, no railings are included in the FE models, although such obstructions are

known to cause major changes in the fluid flow with subsequent increase of the aerodynamic forces acting on the bridge deck.

The first vortex-shedding simulations carried out are based on the model shown in Fig. 6. The mesh is regular unstructured with 3438 eight-noded hexahedral elements and 2×3564 nodes, and the element height nearest to the deck (h_b) is 1000 mm, thus this is a coarse mesh with no attempt to model the boundary layer.

From the prescribed initial conditions, as described in Section 2, and with 8 m/s inflow velocity corresponding to $\mathrm{Re} = 1.65 \times 10^7$, the fluid solution approaches a steady oscillatory state after approximately a dimensionless time $t^* = tU/B = 8$. It exhibits a well-developed vortex street with a wake spacing ratio of 0.39 ($= 3.2D/8.3D$), vortices being shed with a frequency of 0.19 Hz in an alternating pattern from opposite sides of the fixed bridge deck, as shown in Fig. 7. This is equivalent to a prediction $\mathrm{St} = 0.11$, which agrees with the model tests (Larose, 1992) and within the range of St values of 0.08 – 0.15 obtained during full-scale measurements (Frandsen, 2001). Fig. 7 shows generated flow features such as the separation bubble at the top flange of the leading edge and the "dead-air" region in the near-wake (low velocities). Although the no-slip condition seems to be accounted for, the velocity vector profiles show no evidence that the boundary layer is modelled realistically. These results, generated on an extremely coarse mesh, nevertheless demonstrate the capability of the solver to develop periodic shedding. The model (mesh 1) is improved in the following model (mesh 2) by increasing the number of elements in the wake and near the deck surfaces. The fluid domain ($3.2B \times 6.5B$) is meshed with 3420 six-noded triangular prism elements and 2×1884 nodes (mesh 2), as shown in Fig. 8. Note that the total number of elements is similar to the initial model (mesh 1), but the number of nodes has been reduced by approximately a factor of 2 due to the irregular unstructured mesh. The simulation is started from $t = 0$ with $u_x = 8$ m/s, $v_y = 0$ and $p = 0$ as initial conditions at every nodal point in the FE model. From this nonphysical initial condition, the solution approaches a steady state oscillatory condition yielding a value of $\mathrm{St} = 0.28$ using a fixed

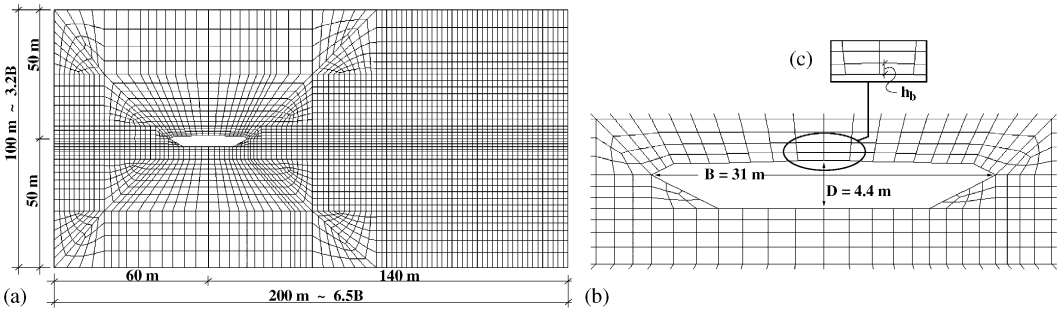

Fig. 6. Discretization of the fluid region (mesh 1) around the suspension bridge of the Great Belt East. Mesh with 3438 elements and 2×3564 nodes. (a) whole mesh, (b) close-up and (c) element size near deck surface, $h_b = 1000$ mm.

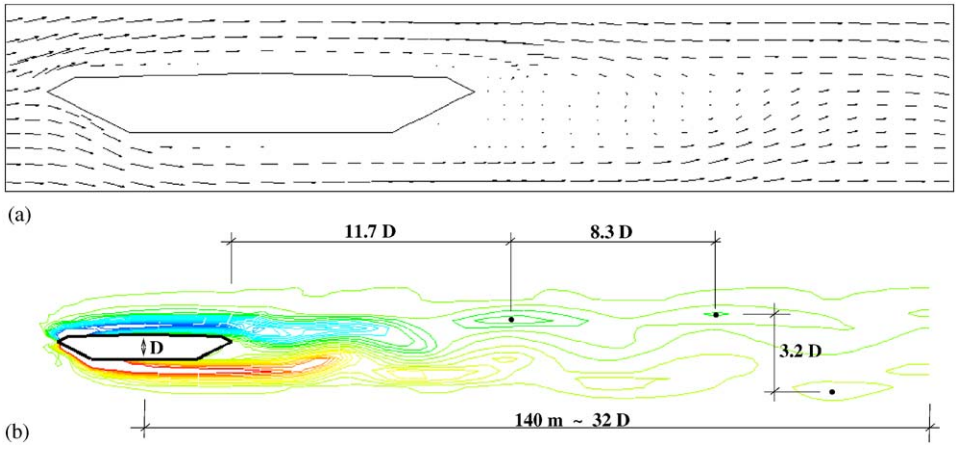

Fig. 7. Flow solution (mesh 1) corresponding to an $\mathrm{Re} = 1.65 \times 10^7$ at $t^* = 38.2$, with a fixed time increment: $\Delta t^* = 0.005$. (a) Velocity vector field and (b) vorticity contours.

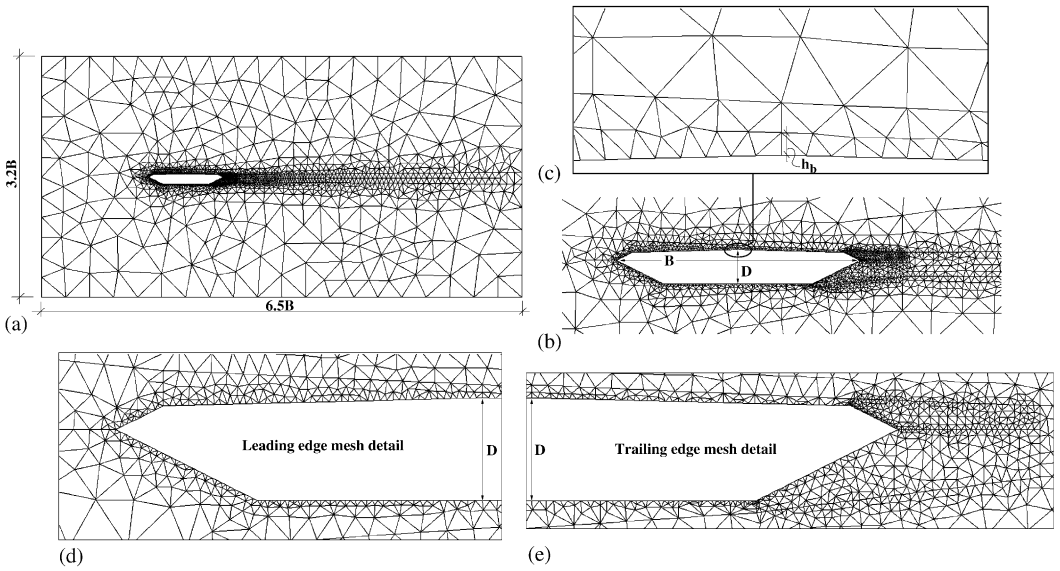

Fig. 8. Discretization of the fluid region (mesh 2) around the suspension bridge of the Great Belt East. Mesh with 3420 elements and 2×1884 nodes. (a) Whole mesh, (b) close-up, (c) element size near deck surface, $h_b = 245$ mm, (d) leading edge and (e) trailing edge.

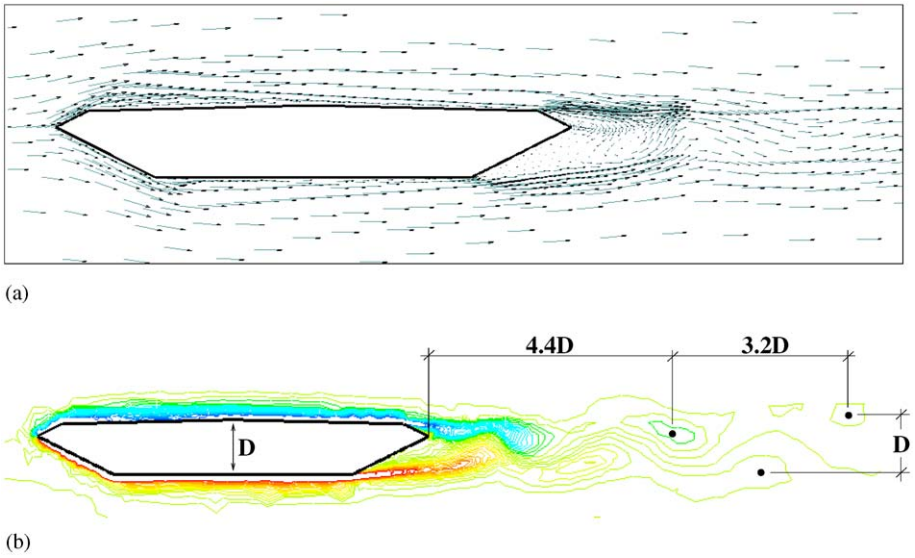

Fig. 9. Flow solution (mesh 2) corresponding to an $\mathrm{Re} = 6.2 \times 10^6$ at $t^* = 23.2$, with a fixed time increment: $\Delta t^* = 0.005$. (a) Velocity vector field and (b) vorticity contours.

time increment $\Delta t^* = 0.005$. This is at some variance to the experimentally recorded St of 0.08 – 0.15. The discrepancy is possibly due to not capturing the real turbulent flow. This result is also further from the experimental result than the value of 0.11 obtained using the more coarse model of mesh 1. The model of mesh 2 was also tested for other Reynolds numbers. Fig. 9 shows a simulation at $\mathrm{Re} = 6.2 \times 10^6$ resulting in a value of $\mathrm{St} = 0.26$. Also for this model the velocity profiles near the deck surface again show no indication that the boundary layer is modelled realistically. An analysis with ramped inflow velocities was also carried out. This revealed the model to be sensitive to initial conditions. Some initial conditions were observed to cause a phenomenon similar to numerical locking, i.e., when one of the variables at an interior node (or nodes) is unable to change. For those initial conditions, the model did not develop a periodic wake but merely exhibited a dead-air region behind the bridge. For those initial conditions that did produce wakes, the wake

spacing ratio of 0.31 (= $D/3.2D$) had decreased compared to the 0.39 ratio obtained from mesh 1, as illustrated in Fig. 9. A sensitivity study on reducing the time increment revealed no significant change in the shedding frequency. The numerical estimated mean aerodynamic coefficients (mesh 2) were found to be around $C_D = 0.51$ and $C_L = -0.08$. The drag coefficient compares well with the drag ($C_D = 0.54$) of the section model test (part of main span; 1:80) (DMI and SINTEF, 1993b). However, the lift coefficient differs by 20% but compares well with the lift coefficient ($C_L = -0.08$) of the Taut strip (main span; 1:300) model (Larose, 1992). Many other models with increased mesh density have been tested (Frandsen, 1999) but are not presented herein as the model of mesh 2 suffices for the simulation of the aeroelastic phenomenon of flutter.

5. Flutter instability

In the following, we investigate the ability of the FE model to simulate classical flutter. It is shown that the mechanism of flutter are independent of the much higher frequency bluff body shedding phenomenon. Furthermore, it is also recognized that the flat-plate flutter theory of Theodorsen (1935) gives comparatively accurate solutions despite the assumption of inviscid flow, suggesting that accurate modelling of the boundary layer may not be so critical for this aeroelastic phenomenon compared to for example modelling of vortex-induced oscillations.

Flutter instabilities occur at high wind speeds as a result of the dominance of self-excited aerodynamic forces. These always involve torsional motions, and may also involve vertical bending motions. Fig. 10 shows the characteristic response due to *classical flutter*, which involves a 2-D bluff body able to move, with restraint, in both vertical translation and rotation. Classical flutter occurs at a wind velocity that has a motion-induced wind load at which the vertical and torsional vibration modes couple. The risk of flutter-induced vibrations is significant when the torsional natural frequency is only slightly larger than the vertical natural frequency, which is often the case on slender long-span bridge decks. For a flat plate or a thin aerofoil, this is a clearly defined phenomenon which requires a coupled oscillation; i.e., simultaneous vertical and torsional motion at a specific relative amplitude and phase. The potential energy input by the aerodynamic forces in flutter is very large and consequently the rise in amplitude is known to be rapid if the flutter limit is reached with catastrophic effects. In contrast to vortex-induced oscillations, this phenomenon is also insensitive to structural damping, as illustrated in Fig. 10. Moreover, the global coupled flutter motion is unaffected by vortex shedding although vortex shedding does occur as would be expected for any bluff section. An acceptable flutter limit is one of the principal design criteria for long-span bridges and Scanlan's theory of flutter derivatives is widely used to estimate this (Scanlan and Tomko, 1971). The solution of the flutter speed based on 2-D inviscid flat-plate theory was established by Theodorsen (1935). It was later approximated by Selberg (1961) for bridge decks as

$$\frac{V_f}{f_\alpha B} = 5.246\sqrt{\left(\frac{m}{\rho_{\text{air}} B^2}\frac{r}{B}\right)\left(1-\left(\frac{f_v}{f_\alpha}\right)^2\right)}, \tag{12}$$

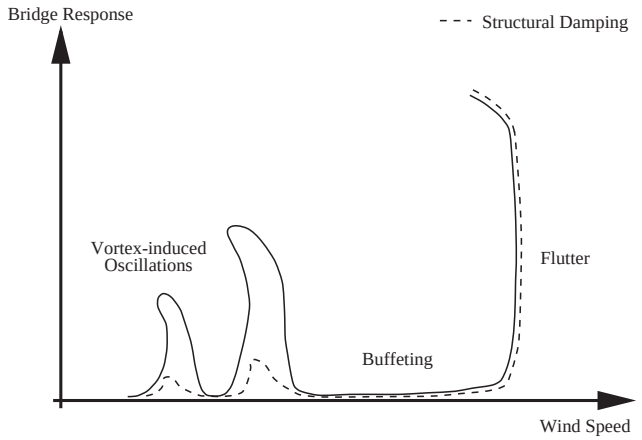

Fig. 10. Sketch of wind-induced aeroelastic phenomena.

where V_f is the critical flutter wind speed. The mass is denoted by m and the radius of gyration $r = \sqrt{I_m/m}$, where I_m is the mass moment of inertia and B is the width of the bridge. The vertical natural frequency is denoted f_v and the torsional natural frequency f_α, respectively. The separation of the torsional natural frequency of the structure and the vertical natural frequency has a major effect on the critical speed. The flutter limit prediction by Selberg is known to give reliable and good predictions for practical box-girder cross-sections compared to wind tunnel test results, provided f_v/f_α is not too close to unity.

In the wind tunnel, the flutter limit behavior of a particular cross-section is measured using either prescribed motion or free oscillation experiments with section models. From these experiments, a set of frequency-dependent flutter derivatives are obtained from which the critical flutter velocity of the full-scale structure may be deduced. By contrast, the numerical flutter experiments described herein are all time-domain analyses, with self-excitation arising naturally from forward integration of the nonlinear field equations. This extends the conventional approach of the flutter derivative formulation (Scanlan and Tomko, 1971), which is based on prescribed motion and linearization of the aerodynamic forces. Essentially, Scanlan's theory provides a means of scaling the wind-tunnel experimental results to predict the flutter stability of the full-scale structure. However, it cannot predict the results of experiments a priori in the manner that the FE approach is endeavoring to do. In the present flutter simulations, a spring- and dashpot-supported structure is added to the fluid model of Figs. 6 and 8 using four-noded isoparametric shell elements. The deck model is shown in Fig. 11. Lumped masses were applied to the structure to simulate the mass per unit length and mass moment of inertia per unit length of the full-scale structure, and the spring stiffnesses were ascribed to give the correct natural frequencies in the fundamental symmetric flexural and torsional modes (Fig. 12). The torsional rigidity of the deck is sufficiently high that this required the vertical springs to be placed on wind-transparent 'out-riggers' outside the cross-section. Horizontal motion was restrained by a horizontal spring attached at the intersection of four stiff, massless struts meeting at the shear center. The structural properties used in the flutter suspension bridge analyses are listed in Table 1. The initial conditions in the flutter analyses must be treated carefully. The instantaneous application of the full wind speed to an initially stationary structure leads to large transient initial motions from which it is difficult to extract definitive conclusions about the stability of small oscillations. To eliminate this problem, structural damping values are set to near-critical values for the first few seconds of the simulation until the structure settles into a near-stationary configuration. The damping values are then changed to their estimated full-scale values. In this case they have prescribed values of 1% and 0.6% logarithmic decrement for vertical and torsional modes, respectively. The subsequent response under further forward integration was then observed to determine if the amplitude of small residual oscillations decay or grow. The observed self-excited oscillatory behavior predicted by *Spectrum* followed the flutter motion predicted by flat-plate theory (Theodorsen, 1935), as shown in Fig. 13. During a flutter motion, it can be

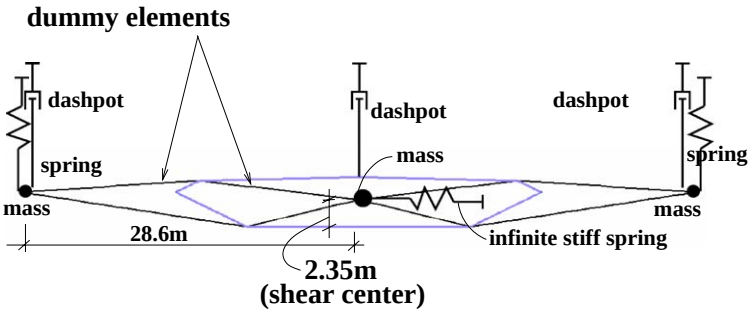

Fig. 11. Flutter deck model used in FE simulations.

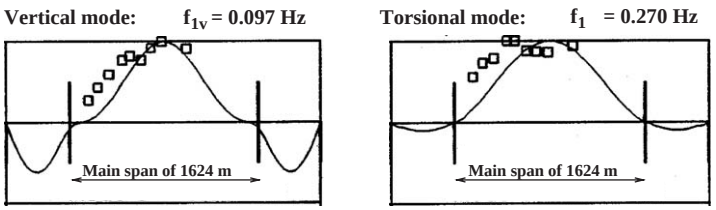

Fig. 12. Flutter modes: □, full-aeroelastic model; –, taut strip model. The symmetric first vertical and torsional modes of vibrations, after Larose (1992).

Table 1
Full-scale properties of the Suspension Bridge (DMI and SINTEF, 1993b) used in the first symmetric flutter mode simulations

Natural vertical frequency (f_{1v}) (Hz)	0.097
Natural torsional frequency ($f_{1\alpha}$) (Hz)	0.270
Mass per unit length (m) (kg/m)	23 687
Equivalent spring stiffness for vertical bending mode per unit length (k_v) (N/m^2)	8785.06
Mass moment of inertia about shear center per unit length (I_m) (kgm^2/m)	2.501×10^6
Equivalent spring stiffness for torsional mode per unit length (G_α) (Nm/m)	7.194×10^6

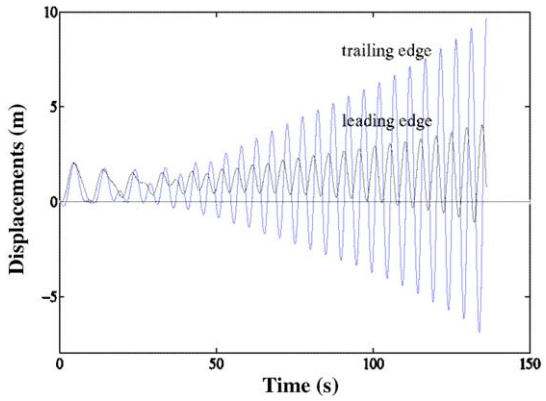

Fig. 13. *Spectrum* prediction of the flutter motion showing time histories of vertical displacements at leading and trailing edge (mesh 1). Inflow velocity of 50 m/s.

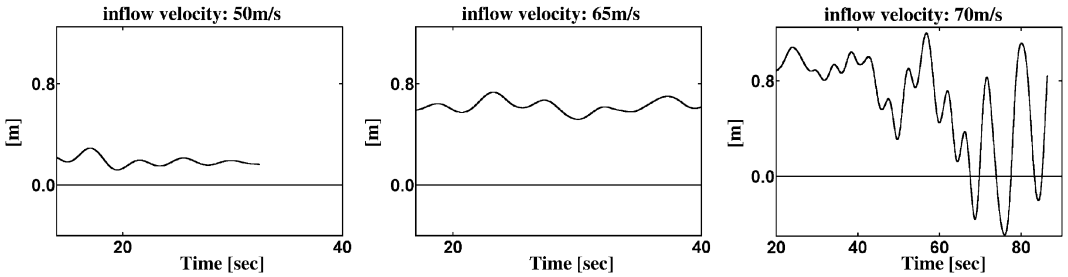

Fig. 14. Flutter solution (mesh 2). Histories of vertical displacements at the downwind out-rigger.

observed that the tip (or near) leading edge acts as the point of rotation with much larger amplitudes present at the trailing edge. This is in contradiction to the flutter eigenvector suggested in Hay (1992), whose argument is based on quasi-static considerations and does not take full account of dynamic effects. As mentioned previously, rather than aiming to determine flutter derivatives, the intention here is to determine the flutter limit directly by forward integration of the field equations. The self-excited flutter solutions related to meshes 1 and 2 are shown in Figs. 13 and 14. The coarsest model solution (mesh 1) shown in Fig. 13 suggest a flutter limit of around 50 m/s. Fig. 14 shows some selected displacement histories at a variety of wind speeds for the improved boundary layer model (mesh 2). These results suggest that the fluid model of mesh 1 is inadequate as the model of mesh 2 predicts a flutter velocity of around 70 m/s close to the 70 – 75 m/s predicted by the original wind tunnel tests conducted on the section model, taut strip and full-aeroelastic models (as listed in Table 2). A shapshot of the associated mesh and pressure contours is also shown in Fig. 15 at a time when the flutter limit of 70 m/s is reached. Mesh dependency of the flutter predictions is therefore evident, and in this case at least, the refined boundary layer model although still relatively coarse model (mesh 2)

Table 2
Flutter limit predictions from various methods for the Great Belt East Suspension bridge

Source	Flutter limit (m/s)	Forced	Self-excited
FEs (mesh 2), without vanes			
Spectrum analysis	70		×
FEs (Fig. 17), with vanes			
Spectrum analysis	65		×
FEs (14 805 nodes)			
(Selvam et al., 2002)	69		×
Finite volume (40 000 cells)			
(Jenssen and Kvamsdal, 1999)	70	×	
Discrete vortices (Larsen and Esdahl, 1998)	72	×	
Discrete vortices (Frandsen, 1999)	65		×
Section model, 1:80, without wind screens			
(DMI and SINTEF, 1993b)	74		×
Section model, 1:80, with wind screens			
(DMI and SINTEF, 1993a)	67		×
Taut strip model, 1:300 (Larose, 1992)	72	×	
Full-aeroelastic model, 1:200			
(DMI and SINTEF, 1992)	70–75		×
Approximation (Selberg, 1961)	75	—	—

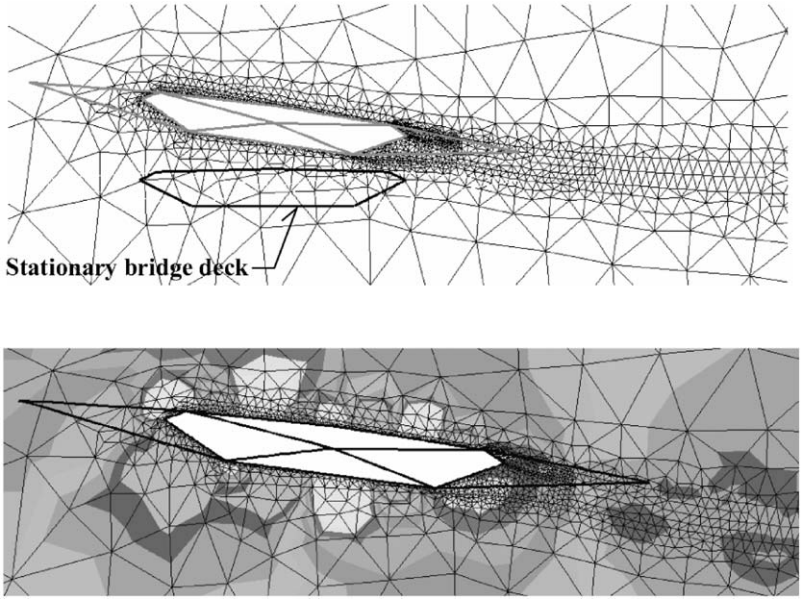

Fig. 15. Snapshot of mesh deformation and pressure contours overlaying the deformed mesh (enlarged by a factor of five). Inflow velocity of 70 m/s.

appears to be giving the more accurate predictions in comparison with the model of mesh 1. Although mesh dependency does exist for this flow regime, it was found to be less sensitive to boundary layer effects compared to the vortex-induced oscillation analyses, as described by Frandsen (1999). This also follows the fairly accurate inviscid flat-plate theory of Theodorsen (1935). Other unstructured models (Frandsen, 1999) were also tested in order to ensure convergence in the numerical solution. In contrast to the FDM, the unstructured grid used in the FE analysis do not include a systematic convergence check. Therefore, it is not possible to conclude with the same certainty if the FE solutions presented has converged. However, comparing solutions (Frandsen, 1999) from the different FE layouts relative to the flutter limit of the physical model tests do guide one to believe that the models used, may be close to what is required for this type of

flow simulation, that is about 1884 nodes in an irregular unstructured grid. Furthermore, it should be noted that the prescribed motion and free oscillation wind tunnel tests in general appear to result in similar stability limits, even though some discrepancies are known to be present when comparing aerodynamic derivatives from the two approaches. For example, the discrete-vortex model did display a significant discrepancy in the predicted flutter limit (Table 2). The FE predictions of *Spectrum* are also in reasonable agreement with numerical flutter limit predictions of other investigators listed in Table 2. For example, Selvam et al. (2002) predicted a self-excited flutter limit of 69 m/s. Their results are based on FE large eddy simulation with a rotating domain which includes a regular unstructured grid of 14 805 nodes. Further we also note that Jenssen and Kvamsdal (1999) are using high-density grids resulting in a requirement for parallel processing. The models used in the *Spectrum* flutter analysis indicate that this may not be needed. At 70 m/s the flexural–torsional oscillations of the *Spectrum* analysis (mesh 2) predict a frequency of about 0.22 Hz which may be compared with the still-air uncoupled fundamental frequencies of 0.097 and 0.27 Hz in flexure and torsion, respectively. A discrete-vortex model developed by Walther (1994) was applied for comparison reasons. In contrast to the flutter limit of 72 m/s based on prescribed motion, the self-excited discrete-vortex model predicted a flutter limit of 65 m/s and a coupling frequency of 0.25 Hz. This is somewhat a lower flutter limit and lower period in comparison with the other methods (Table 2). The reason for this discrepancy is not clear. In agreement with the FE simulation, Jenssen and Kvamsdal (1999) also found that the dominant mode was the torsional motion response with a coupling frequency of 0.21 Hz. Periodic vortex shedding did occur in these simulations as would be expected from such a bluff section (Fig. 16), with a frequency of around 4.4 Hz corresponding to a Strouhal number, St of 0.28. This was also obtained for the flow around the bridge when held in a stationary position (mesh 2). In the time history of Fig. 16, high-frequency signals can be observed on the lower-frequency flutter motion. These signals correspond to the vortex-shedding frequency. The low-frequency flexural–torsional motions are therefore the result of a different aerodynamic effect than vortex-induced bridge vibrations, see Frandsen (1999) for further discussion. Further, we note when the flutter limit is reached, the structure controls the fluid flow. Furthermore, in the *Spectrum* simulations, large static displacements were induced during the initial heavily damped simulations, indicating an over-estimation of the static lift and moment, a result perhaps attributable to the absence of deck furniture from the numerical model. In this context, it appears that flow obstructions such as wind screens (DMI and SINTEF, 1993a) decrease the flutter limit (Table 2). It should also be mentioned that guide vanes were installed on the bridge when the construction were completed, aiming to suppress large vortex-induced vibrations experienced full scale (Frandsen, 2001). Some FE simulations were carried out for the bridge deck with vanes to test the effect of vanes on the flutter limit. The fluid and the deck model are shown in Figs. 17 and 18. Guide-vane surfaces constructed of shell elements were added to the bridge model, attached via stiff four-noded quad elements through which the flow is free to pass. A no-slip condition on vane surfaces was prescribed. The vertical response histories for the models with and without vanes are presented in Fig. 19 showing that the model

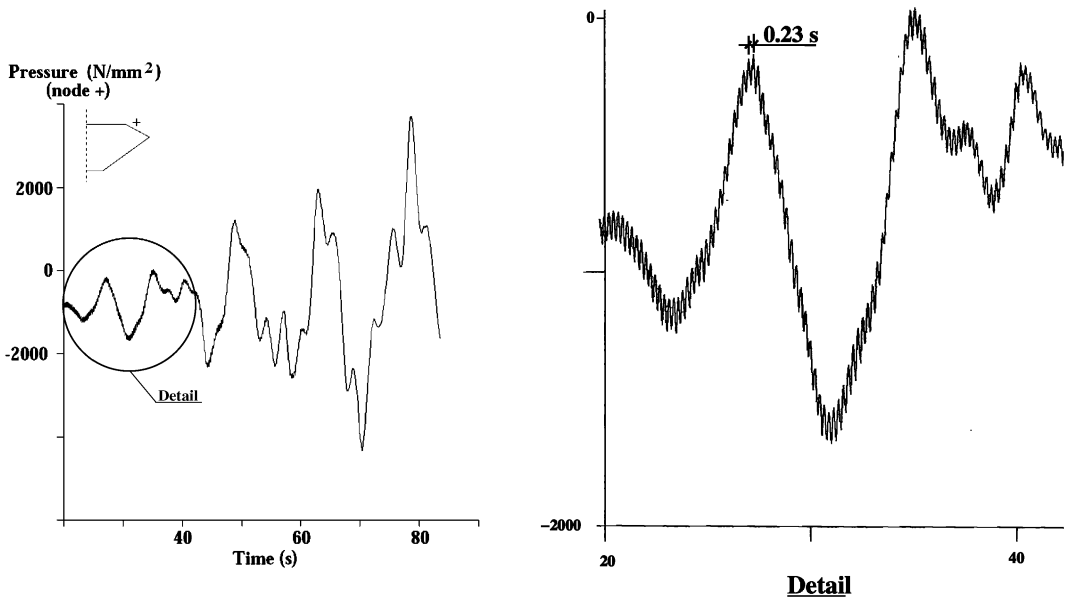

Fig. 16. Pressure history near trailing edge for the lower frequency flutter motion. Details of the high-frequency components equivalent to the vortex shedding are also shown. Inflow velocity of 70 m/s.

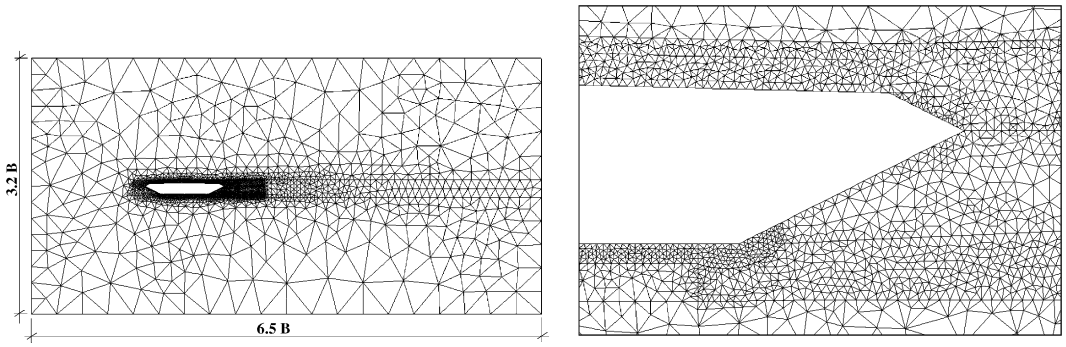

Fig. 17. FE model with guide vanes. Mesh contains 9856 elements and 2×4994 nodes. Mesh detail at trailing edge is shown.

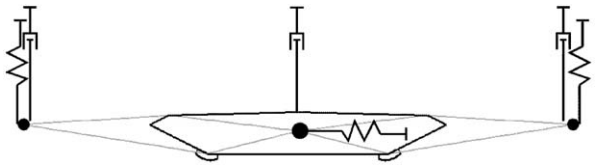

Fig. 18. Location of springs, lumped masses and dashpots in the flutter deck model with vanes.

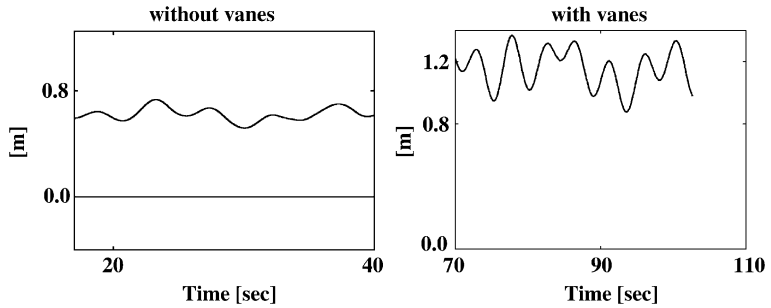

Fig. 19. Comparison of the time histories of vertical displacements at the downwind rigger with and without vanes. Inflow velocity of 65 m/s.

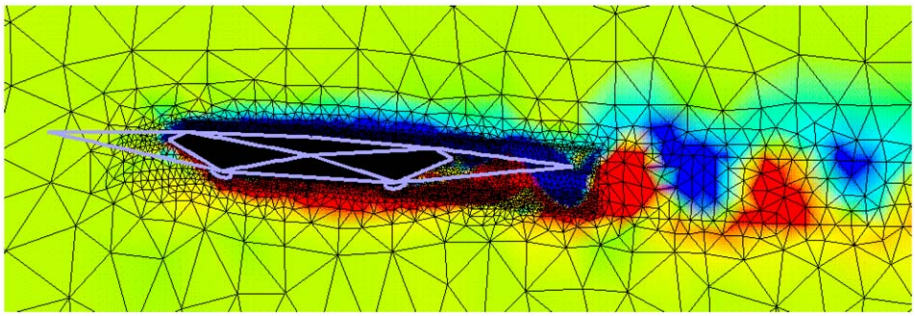

Fig. 20. Snapshot of flutter motion for the deck with vanes.

with vanes is approaching the flutter limit at around 65 m/s. Similar to the flow effects due to railings and wind screens, this type of flow obstruction also causes a decrease of the flutter speed. A snapshot of the flutter motion with an initial condition of 65 m/s is shown in Fig. 20.

Flutter simulations are CPU-intensive analyses. Herein even more so because twice as many nodes were used as required as *Spectrum* allows 3-D elements only. Using a single processor HP C200 workstation, a 40-s simulation for mesh 2 took approximately 40 h using a time step of 0.003 s. The models used, despite the coarseness of the meshes compared to those of other investigators, may be close to what is required for this type of flow simulation. However, higher CPU requirements, but not necessarily parallel processing, than those used here are desirable if the method is to prove to be a viable supplementary tool to the wind tunnel.

6. Conclusions

Long-span bridges require extensive wind tunnel testing. The objective of this research is to determine whether a computational method can lead to a reduction in the number of expensive physical model tests that are currently required to determine the aerodynamic cross-section of a single structure. This study describes the use of a coupled fluid–structure interaction (FSI) finite element (FE) solver. Aerodynamic effects of flutter-bridge motion are investigated using fluid and structural two-dimension FEs on moving nonadaptive grids. The moving interface between fluid and structure is modelled through the arbitrary Lagrangian–Eulerian (ALE) formulation.

First, simulation of fluid flow around a fixed bridge deck was simulated. The FE model was validated using different meshes for a range of high Reynolds numbers. Time-domain vortex-shedding analysis was presented. Some questions as to model accuracy were raised due to a discrepancy in Strouhal number compared to physical experiments. The reason being that the turbulent flow around the fixed deck problem was not captured reliably with the present viscous FE solver. However, it was shown, that the mechanisms of flutter are independent of the much higher-frequency bluff body shedding phenomenon and was therefore not explored any further in this study.

Second, flutter simulations were presented showing the ability of the FE model to self-excite into flexural–torsional flutter. The FE simulations showed that, when the flutter limit is reached, the structure controls the fluid flow. The flutter limit of the long-span bridge deck was found to be in good agreement with the wind tunnel results and other numerical methods. Furthermore, it is also recognized that the flat-plate flutter theory of Theodorsen (1935) gives comparatively accurate solutions despite the assumption of inviscid flow, suggesting that accurate modelling of the boundary layer may not be so critical for this aeroelastic phenomenon. The models used, despite the laminar flow assumption and the coarseness of the meshes compared to those of other investigators, may be close to what is required for this type of flow simulation, that is about 1900 nodes in an irregular unstructured grid. However, a higher CPU requirement, but not necessarily parallel processing, than those used here is desirable if the FE ALE approach is to prove to be a viable supplementary tool to the wind tunnel.

In conclusion, prediction of flutter instability for sharp edge bridge decks does not appear sensitive to turbulence and three-dimensional flow structure modelling.

Acknowledgements

I am very grateful to Prof. C. Dalton, Department of Mechanical Engineering, University of Houston, for the many valuable comments to the manuscript.

References

Anju, A., Maruoka, A., Kawahara, M., 1997. 2-D fluid–structure interaction problems by an arbitrary Lagrangian–Eulerian finite element method. International Journal of Computational Fluid Dynamics 8, 1–9.

Ansys Inc., 1999. Spectrum Solver (Version 2.0) Command Reference and Theory Manual. Ansys Inc., USA (Spectrum was commercially available in 1993–1999 and is a registered trademark of Ansys Inc.).

Brar, P.S., 1997. Numerical calculation of bluff body flutter derivatives via computational fluid dynamics. Ph.D. Thesis, The John Hopkins University, Baltimore, MD, USA.

Bruno, L., Khris, S., Marcillat, J., 2001. Numerical simulation of the effect of section details and partial streamlining on the aerodynamics of bridge decks. Journal of Wind and Structures 4, 315–332.

Chorin, A.J., 1989. Numerical study of slightly viscous flow. Journal of Fluid Mechanics 57(4), 785–796. 1973.

Dahle, L.A., Reed, K., Aarsnes, J.V., 1990. Model tests with submerged floating tube bridges. In: Krokeborg, J. (Ed.), Proceedings of the Second Symposium on Strait Crossings. Balkema, Trondheim, Norway.

De Foy, B., 1998. Unsteady incompressible flow solver with optimised operators. Ph.D. Thesis, Cambridge University, Department of Engineering, Cambridge, England.

DMI and SINTEF, 1993a. Wind-tunnel tests. Storebælt East Bridge. Suspension bridge. Section model tests, II. Technical Report 92063.00.01, Danish Maritime Institute, Lyngby, Denmark (Used with permission from Storebælt A/S).

DMI and SINTEF, 1993b. Wind-tunnel tests. Storebælt East Bridge. Tender evaluation, suspension bridge. Alternative sections. Section model tests, I. Technical Report 91023-10.00. Revision 0., Danish Maritime Institute, Lyngby, Denmark (Used with permission from Storebælt A/S).

Donea, J., Fasoli-stella, P., Giuliani, S., 1977. Lagrangian and Eulerian finite element techniques for transient fluid–structure interaction problems. Transactions Fourth SMIRT Conference, San Fransisco, 15–19 August 1977, USA (Paper B1/2).

Dowell, E.H., Crawley, E.F., Curtiss Jr., H.C., Peters, D.A., Scanlan, R.H., Sisto, F., 1995. A Modern Course in Aeroelasticity, 3rd Edition. Kluwer Academic Publishers, Dordrecht.

Dyrbye, C., Hansen, S.O., 1997. Wind Loads on Structures. Wiley, New York.

Felippa, C.A., Park, K.C., 1980. Staggered transient analysis procedures for coupled mechanical systems: formulation. Computer Methods in Applied Mechanics and Engineering 24, 61–111.

Frandsen, J.B., 1999. Computational fluid–structure interaction applied to long-span bridge design. Ph.D. Thesis, Cambridge University, Engineering Department, England.

Frandsen, J.B., 2001. Simultaneous pressures and accelerations measured full-scale on the Great Belt East suspension bridge. Journal of Wind Engineering and Industrial Aerodynamics 89, 95–129.

Fujiwara, A., Kataoka, H., Ito, M., 1993. Numerical simulation of flow field around an oscillating bridge using finite difference method. Journal of Wind Engineering and Industrial Aerodynamics 46–47, 567–575.

Fung, Y.C., 1993. An Introduction to the Theory of Aeroelasticity. Dover Publications, New York.

Gilbert, D., 1826. On the mathematical theory of suspension bridges, with tables for facilitating their construction. Philosophical Transactions of the Royal Society of London 116, 202–218.

Hay, J., 1992. Response of Bridges to Wind. HMSO, TRL, Department of Transport, London, UK.

Hilber, H.M., Hughes, T.J.R., Taylor, R.L., 1977. Improved numerical dissipation for time integration algorithms in structural dynamics. Earthquake Engineering and Structural Dynamics 5, 283–292.

Hughes, T.J.R., Brooks, A.N., 1979. A Multi-dimensional Upwind Scheme With no Crosswind Diffusion. ASME, New York.

Hughes, T.J.R., Franca, L.P., Hulbert, G.M., 1989. A new finite element formulation for computational fluid dynamics: viii. the Galerkin least squares method for advective–diffusive equations. Computer Methods in Applied Mechanics and Engineering 73, 173–189.

Hughes, T.J.R., Liu, W.K., Zimmerman, T.K., 1981. Lagrangian–Eulerian finite element method incompressible viscous flows. Computer Methods in Applied Mechanics and Engineering 29 (1), 329–349.

Jenssen, C.B., 1998. Industrial use of large eddy simulation. In: Emerson, D.R., et al. (Ed.), Parallel Computational Fluid Dynamics. Recent Development and Advances using Parallel Computers. Elsevier Science B.V., The Netherlands, pp. 587–592.

Jenssen, C.B., Kvamsdal, T., 1999. Computational methods for fsi-simulations of slender bridges on high performance computers. In: Kvamsdal, T., et al. (Ed.), Computational Methods for Fluid–Structure Interaction. Tapir Forlag, Trondheim, Norway, pp. 31–40.

Karniadakis, G., Sherwin, S.J., 1999. Spectral/hp Element Methods for CFD. Oxford University Press, Oxford.

Kuroda, S., 1997. Numerical simulation of flow around a box girder of a long span suspension bridge. Journal of Wind Engineering and Industrial Aerodynamics 67–68, 239–252.

Kvamsdal, T., Jenssen, C.B., Okstad, K.M., Amundsen, J., 1999. Fluid–structure interaction for structural design. In: Kvamsdal, T., et al. (Ed.), Computational Methods for Fluid–Structure Interaction. Tapir Forlag, Trondheim, Norway, pp. 212–238.

Larose, G.L., 1992. The Response of a Suspension Bridge Deck to Turbulent Wind: the Taut Strip Model Approach. M.Eng.Sc., The University of Western Ontario, London, Ont., Canada, March.

Larsen, A. (Ed.), 1992. Aerodynamics of Large Bridges. Balkema, Rotterdam, Netherlands.

Larsen, A., Esdahl, S. (Eds.), 1998. Bridge Aerodynamics. Balkema, Rotterdam, Netherlands.

Larsen, A., Jacobsen, A.S., 1992. Aerodynamic design of the great belt east bridge. In: Larsen, A. (Ed.), Aerodynamics of Large Bridges. Balkema, Rotterdam, Netherlands, pp. 269–283.

Lee, J.S., Lee, S.S., Kim, J.D., Kim, H.M., Koh, H.M., Jeong, U., Park, S.H., Seong, T.Y., 1995. The aerodynamic stability analysis system of the large-scale structures. Technical Report, CAE Group, Division of Systems Application of the Systems Engineering Research Institute and Seoul National University, Civil Engineering Department, Republic of Korea, December.

Leonard, A., 1980. Review. Vortex methods for flow simulations. Journal of Computational Physics 37, 289–335.

Li, L., Sherwin, S., Bearman, P., 2002. A moving frame of reference algorithm for fluid/structure interaction of rotating and translating bodies. International Journal for Numerical Methods in Fluids 38, 187–206.

Mendes, P.A., Branco, F.A., 1998. Numerical wind studies for the Vasco da Gama Bridge, Portugal. Structural Engineering International 8 (2), 124–128.

Mendes, P.A., Branco, F.A., 1999. Analysis of fluid–structure interaction by an arbitrary Lagrangian–Eulerian finite element formulation. International Journal for Numerical Methods in Fluids 30, 897–919.

Morgenthal, G., McRobie, A., 2002. A comparative study of numerical methods for fluid–structure interaction analysis in long-span bridge design. Journal of Wind and Structures 5 (2–4), 101–114.

Noh, W.F., 1964. CEL A time-dependent two-space-dimensional, coupled Eulerian–Lagrange code. Methods in Computational Physics 3, 117–179.

Nomura, T., Hughes, T.J.R., 1992. An arbitrary Lagrangian–Eulerian finite element method for interaction of fluid and rigid body. Computer Methods in Applied Mechanics and Engineering 95 (11), 115–138.

Okstad, K.M., Mathisen, K.M., 1998. Fluid–structure interaction simulation of submerged floating tunnels. Part 2: 2D section models. Technical Report R-11-98, The Norwegian University of Science and Technology, Department of Structural Engineering, Trondheim, Norway, April.

Onyemelukwe, O.U., 1993. Computer simulation of wind effects on bridges and other bluff bodies. Ph.D. Thesis, University of Pittsburgh, USA (Volumes I and II).

Onyemelukwe, O.U., Roy, B., Bosch, H., 1998. Coupling of the finite-difference method and the boundary element—dual reciprocity method for wind flow simulation. Journal of Wind Engineering and Industrial Aerodynamics 77–78, 631–641.

Parkinson, G.V., 1989. Phenomena and modelling of flow-induced vibration of bluff bodies. Progress Aerospace Sciences 96, 169–224.

Pugsley, A., 1957. The Theory of Suspension Bridges. Edward Arnold Ltd., London.

Remseth, S., Leira, B., Okstad, K.M., Mathisen, K.M., Haukås, T., 1999. Dynamic response and fluid/structure interaction of submerged floating tunnels. Computers and Structures 72, 659–685.

Robertson, I., Li, L., Sherwin, S., Bearman, P., 2003a. A numerical study of rotational and transverse galloping rectangular bodies. Journal of Fluids and Structures 17 (5), 681–699.

Robertson, I., Sherwin, S., Bearman, P., 2003b. Flutter instability prediction techniques for bridge deck sections. International Journal for Numerical Methods in Fluids 43 (10–11), 1239–1256.

Robertson, I., Sherwin, S., Bearman, P., 2003c. Prediction of rotational galloping of rectangular and semi-circular leading edge sections. Journal of Flow Turbulence and Combustion, in press.

Sarpkaya, T., 1989. Computational methods with vortices, The 1988 Freeman Scholar lecture. Journal of Fluid Mechanics 111, 5–52.

Scanlan, R.H., 1981. On state of the art methods for calculations of flutter, vortex-induced and buffeting response of bridge structures. Technical Report FHWA/RD-80/050, National Technical Information Service, Springfield, Virginia, USA.

Scanlan, R.H., Tomko, J.J., 1971. Airfoil and bridge deck flutter derivatives. ASCE Journal of Engineering Mechanics Division 97, 1717–1737.

Selberg, A., 1945. Design of suspension bridges. Number 1. Det KGL. Norske videnskabers selskabs skrifter.

Selberg, A., 1961. Oscillation and aerodynamic stability of suspension bridges. Technical Report Acta Polytechnica, Scandinavica Ci13.

Selvam, R.P., 1998. Computational procedures in grid based computational bridge aerodynamics. In: Larsen, A., Esdahl, S. (Eds.), Bridge Aerodynamics. Balkema, Rotterdam, Netherlands, pp. 327–336.

Selvam, R.P., Govindaswamy, S., Bosch, H., 2002. Aeroelastic analysis of bridges using FEM and moving grids. Journal of Wind and Structures 5 (2–4), 257–266.

Simiu, E., Scanlan, R.B., 1996. Wind Effects on Structures. Wiley, New York.

Smagorinsky, J., 1993. In: Galperin, B., Orszag, S.A. (Eds.), Large Eddy Simulation of Complex Engineering and Geophysical Flows. Cambridge University Press, Cambridge.

Taylor, I., Vezza, M., 2002. Aeroelastic stability analysis of a bridge deck with added vanes using a discrete vortex method. Journal of Wind and Structures 5 (2–4), 277–290.

Theodorsen, T., 1935. General theory of aerodynamic instability and the mechanism of flutter. Technical Report 496, NACA.

Turbelin, G., Gibert, R.J., 2002. CFD calculations of indicial lift responses for bluff bodies. Journal of Wind and Structures 5 (2–4), 245–256.

Walther, J.H., 1994. Discrete Vortex Method for two-dimensional flow past bodies of arbitrary shape undergoing prescribed rotary and translatory motion. Ph.D. Thesis, The Technical University of Denmark, Department of Fluid Mechanics, Lyngby, Denmark.

Walther, J.H., Larsen, A., 1997. Analytical and discrete vortex models for an oscillating flat plate with trailing edge flap. In: Eighth US National Conference on Wind Engineering. Baltimore, USA CD-ROM.